Effects of $MgSiO_3$ on the crystal growth and characteristics of type-Ib gem quality diamond in Fe-Ni-C system

Zhi-Yun Lu(鲁智云), Yong-Kui Wang(王永奎), Shuai Fang(房帅), Zheng-Hao Cai(蔡正浩), Zhan-Dong Zhao(赵占东), Chun-Xiao Wang(王春晓), Hong-An Ma(马红安), Liang-Chao Chen(陈良超), and Xiao-Peng Jia(贾晓鹏)

Citation: Chin. Phys. B, 2020, 29 (**12**): 128103. DOI: 10.1088/1674-1056/abb800
Journal homepage: http://cpb.iphy.ac.cn; http://iopscience.iop.org/cpb

What follows is a list of articles you may be interested in

Two-step high-pressure high-temperature synthesis of nanodiamonds from naphthalene

Tong Liu(刘童), Xi-Gui Yang(杨西贵), Zhen Li(李振), Yan-Wei Hu(胡宴伟), Chao-Fan Lv(吕超凡), Wen-Bo Zhao(赵文博), Jin-Hao Zang(臧金浩), Chong-Xin Shan(单崇新)

Chin. Phys. B, 2020, 29 (**10**): 108102. DOI: 10.1088/1674-1056/abad1c

Crystallization and characteristics of {100}-oriented diamond with CH_4N_2S additive under high pressure and high temperature

Yong Li(李勇), Debing Tan(谭德斌), Qiang Wang(王强), Zhengguo Xiao(肖政国), Changhai Tian(田昌海), Lin Chen(陈琳)

Chin. Phys. B, 2020, 29 (**9**): 098103. DOI: 10.1088/1674-1056/ab99b9

Effects of microwave oxygen plasma treatments on microstructure and Ge-V photoluminescent properties of diamond particles

Ling-Xiao Sheng(盛凌霄), Cheng-Ke Chen(陈成克), Mei-Yan Jiang(蒋梅燕), Xiao Li(李晓), Xiao-Jun Hu(胡晓君)

Chin. Phys. B, 2020, 29 (**8**): 088101. DOI: 10.1088/1674-1056/ab8db0

Regulation mechanism of catalyst structure on diamond crystal morphology under HPHT process

Ya-Dong Li(李亚东), Yong-Shan Cheng(程永珊), Meng-Jie Su(宿梦洁), Qi-Fu Ran(冉启甫), Chun-Xiao Wang(王春晓), Hong-An Ma(马红安), Chao Fang(房超), Liang-Chao Chen(陈良超)

Chin. Phys. B, 2020, 29 (**7**): 078101. DOI: 10.1088/1674-1056/ab90e8

Influences of grain size and microstructure on optical properties of microcrystalline diamond films

Jia-Le Wang(王家乐), Cheng-Ke Chen(陈成克), Xiao Li(李晓), Mei-Yan Jiang(蒋梅燕), Xiao-Jun Hu(胡晓君)

Chin. Phys. B, 2020, 29 (**1**): 018103. DOI: 10.1088/1674-1056/ab593d

Effects of $MgSiO_3$ on the crystal growth and characteristics of type-Ib gem quality diamond in Fe–Ni–C system*

Zhi-Yun Lu(鲁智云)[1], Yong-Kui Wang(王永奎)[1], Shuai Fang(房帅)[1], Zheng-Hao Cai(蔡正浩)[1], Zhan-Dong Zhao(赵占东)[1], Chun-Xiao Wang(王春晓)[1], Hong-An Ma(马红安)[1,†], Liang-Chao Chen(陈良超)[2,‡], and Xiao-Peng Jia(贾晓鹏)[1,§]

[1] *State Key Laboratory of Superhard Materials, College of Physics, Jilin University, Changchun* 130012, *China*

[2] *Key Laboratory of Materials Physics of Ministry of Education, School of Physics, Zhengzhou University, Zhengzhou* 450001, *China*

(Received 4 July 2020; revised manuscript received 23 August 2020; accepted manuscript online 14 September 2020)

We report the effects of $MgSiO_3$ addition on the crystal growth and characteristics of type-Ib diamonds synthesized in Fe–Ni–C system. The experiments were carried out with pressure at 5.5 GPa, temperature at 1385 °C–1405 °C, and duration of 23.1 h. As $MgSiO_3$ increases from 0.0 wt% to 3.0 wt%, the diamond growth temperature increases from 1385 °C to 1405 °C, the addition of $MgSiO_3$ and the movement of *P*–*T* diagram toward the higher temperature direction result in a series of effects to the Fe–Ni–C system and crystal growth. Firstly, it increases the content of metastable recrystallized graphite and accelerates the competition with the carbon source needed for diamond growth, thus causing the decreased crystal growth rate. Diamond crystals exhibit the combination form of {111}, {100}, {113}, and {110} sectors, the decreased {100} and {113} sectors, dominated {111} sector are all attributed to the higher growth rate in [100] direction caused by the synergy of $MgSiO_3$ and the movement of *P*–*T* diagram. The higher growth rate in [100] direction also increases the metal catalyst and graphite inclusions and leads to the increase of residual tensile stress on the crystal surface. Accompanying with the high growth rate, a higher dissolution rate along [100] and [113] directions than [111] direction occurs at the microstructure and forms the significantly developed (111) stepped growth layer. In addition to the movement of *P*–*T* diagram, the addition of $MgSiO_3$ poisons the catalyst and increases the nitrogen content of diamond from 120 ppm to 227 ppm.

Keywords: diamond, $MgSiO_3$, nitrogen content, recrystallized graphite

PACS: 81.10.Aj, 81.05.ug, 91.60.–x, 07.35.+k **DOI:** 10.1088/1674-1056/abb800

1. Introduction

Diamond holds an important role in jewelry because of its excellent hardness, refractive index, profound historical and cultural connotations.[1,2] In recent years, with the progress of synthetic technology, synthetic diamond has been rapidly applied in the jewelry industry.[3–6] At present, gem quality diamond crystals are produced by high pressure and high temperature (HPHT) and chemical vapor deposition (CVD) methods, of which HPHT method accounts for the main production capacity.[7,8] Metal catalysts such as Fe, Ni, Mn, Co, Ti have been widely used in the synthesis of HPHT diamond,[9–12] natural diamond crystals are believed to mainly originate from silicate or carbonate in the upper mantle, which may partly be affected by some fluids or melts.[13–16] Therefore, based on the traditional HPHT method for synthesizing diamond, researchers began to investigate the nucleation mechanism and characteristics of synthetic diamond in the mantle-like environment.[17–21] Sokol & Pal'yanov (2008) synthesized {111} octahedral diamond crystals in SiO_2–H_2O–C and Mg_2SiO_4–H_2O–C systems at 7.5 GPa and 1600 °C conditions.[18] At conditions of 7 GPa and 1700 °C–1900 °C, Palyanov *et al.* (2017) synthesized {111} octahedron and {100} cubic crystals in Mg–C and $Mg_{0.8}Si_{0.2}$–C systems, respectively, the addition of Si promotes the development of the {111} sector.[22] Ding *et al.* (2020) synthesized {111} crystals with a large number of defects in Fe–Ni–C–$Mg_2Si_3O_8{\cdot}5H_2O$ system under 5.8 GPa–6.3 GPa and 1300 °C–1420 °C conditions.[23] However, diamond samples obtained in those carbonate–silicate–C systems are all micron-sized, this is quite different from the size of natural gem quality diamond crystals, it also causes great difficulties for nitrogen analysis commonly used in gem grade diamonds.[18,24–26] Although the temperature gradient method (TGM) can be used to synthesize gem quality diamond crystals, the Fe–Ni–C system is significantly different from the silicate–carbonate system where natural diamond crystals form. It is worth noting that the native Fe and Ni inclusions have been found in the parent rock and inclusions of natural diamond crystals.[27–29] Therefore, the Fe–Ni–C–silicate system

*Project supported by the National Natural Science Foundation of China (Grant Nos. 51772120, 51872112, and 11804305), the China Postdoctoral Science Foundation (Grant No. 2017M622360), and the Project of Jilin Science and Technology Development Plan (Grant No. 20180201079GX).

†Corresponding author. E-mail: maha@jlu.edu.cn

‡Corresponding author. E-mail: chenlc@zzu.edu.cn

§Corresponding author. E-mail: jiaxp@jlu.edu.cn

may also have implication for the formation of natural gem quality diamond crystals. $MgSiO_3$ coexists with diamond in the form of enstatite in the upper mantle,[30] and its effect on the crystallization of diamond has not been reported. The purpose of this paper is to investigate the influence of $MgSiO_3$ on the crystal morphology, internal characteristics and nitrogen content of synthetic gem grade diamond, and to provide experimental evidence for exploring the formation mechanism of natural diamond in the upper mantle.

2. Material and methods

Diamond crystals were synthesized by the temperature gradient method using a China-type large volume cubic high-pressure apparatus (CHPA) (SPD-6×1200). The experiments were carried out with pressure at 5.5 GPa, temperature at 1385 °C–1405 °C, and duration of 23.1 h. The assembly diagram of the high-pressure anvil and synthetic cavities are shown in Fig. 1. The 99.99% graphite was used as carbon source, the $Fe_{64}Ni_{36}$ alloy was used as the catalyst, and Florisil ($MgSiO_3$) with 99% purity was selected as dopant. The carbon source and $MgSiO_3$ were mixed in different proportions using an analytical balance with precision of 10^{-5} g, and then mixed with 12 h on the mixer to ensure complete mixing. In this paper, the {111} crystal of 1 mm in diameter and with triangular shape is selected as the crystal seed. It is placed on the top of MgO insulating medium, and its top surface is flush with the top of MgO insulating medium. The pressure inside the press chamber is calibrated by the phase transformation of Bi, Ba, and Tl under high pressure. The control accuracy of pressure is ±0.01 GPa. The temperature of the chamber is calibrated by using the input power of the Pt-30% Rh/Pt-6% thermocouple. The synthesis temperature in the chamber is controlled by the heating system of CHPA. The control accuracy of the heating power of CHPA in the process of diamond synthesis is ±1 W, and the corresponding temperature control accuracy is ±1 °C.

After the synthesis process was finished, the catalyst with diamond crystals was placed in the mixed heat solution of H_2SO_4 and HNO_3 (volume ratio 3:1) to remove the metal catalyst and graphite on the crystal surface. The crystals were placed in alcohol and washed with ultrasonic for 15 min to remove the oil contamination on the surface of the crystal. First, the crystal shape, surface characteristics and internal characteristics of the samples were observed by a Leica M205 C optical microscope. The weight of the crystals was measured by an analytical balance with a precision of 10^{-5} g. The crystals in our work exhibits mainly {111} sector, therefore, the (111) crystal face was selected for infrared absorption measurements by using a VERTEX 70-V vacuum micro Fourier transform infrared spectrometer. Each sample was measured with a spectral range of 600 cm^{-1} to 4000 cm^{-1} and a resolution of 2 cm^{-1} and the integral number was 64 times. The Raman spectra were measured on the even (111) surface with a Renishaw in Via-type Raman spectrometer, the system equipped with a telescope with 500× magnification, a 532-nm solid stage laser and the laser power (100 mW at the sample surface) was well below the threshold for thermally induced sample degradation. The spectra were recorded in the wavelength region 600 cm^{-1}–2000 cm^{-1} at interval of 1 cm^{-1} with the spot size about 10 μm. An FEI Magellan 400-type scanning electron microscope (SEM) equipped with an Oxford Max-150-type energy dispersive spectrometer (EDS) was used to investigate the distribution pattern of different elements on the catalyst system. The system worked at 15-kV and 1.6-nA conditions.

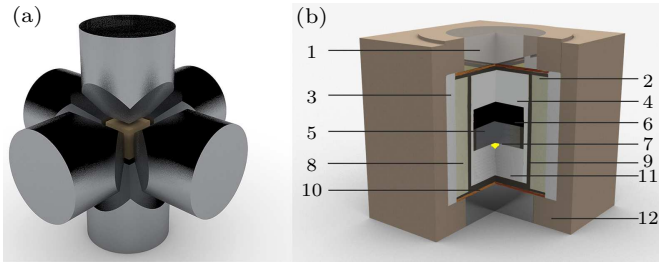

Fig. 1. Schematic diagram of high-pressure anvil, synthetic block and sample assembly. (a) Schematic diagram of high-pressure anvil and synthetic block. (b) Sample assembly for diamond synthesized by HPHT method; 1: steel cap; 2: graphite sheet; 3: dolomite; 4: MgO insulating medium; 5: metal alloy catalyst; 6: graphite carbon source and $MgSiO_3$; 7: crystal seed; 8: NaCl+ZrO_2; 9: graphite heater; 10: copper; 11: MgO insulating medium; 12: pyrophyllite.

3. Results and discussion

3.1. Synthesis conditions and internal characteristics

In the Fe–Ni–C system with 0.0-wt% to 3.0-wt% $MgSiO_3$ doped, the photos of catalyst system before acid treatment and diamond crystals are shown in Figs. 2(a) and 2(b), respectively. Their synthesis conditions are shown in Table 1, and D-1–D-5 are all synthesized under the pressure at 5.5 GPa, among them, D-1 is a medium temperature diamond crystal synthesized at 1385 °C without $MgSiO_3$ doping. D-2–D-5 are medium temperature crystals grown by doping 1.0-wt%, 1.4-wt%, 2.0-wt%, 3.0-wt% $MgSiO_3$, respectively. It can be seen that with the increase of $MgSiO_3$ doping ratio, the growth temperature of the corresponding crystal changes from 0.0-wt%, 1.0-wt%, 1.4-wt% $MgSiO_3$ at 1385 °C to 2.0-wt% $MgSiO_3$ at 1395 °C, and then to 3.0 wt% of $MgSiO_3$ at 1405 °C. It indicates that doping $MgSiO_3$ makes the *P*–*T* diagram of diamond growth move toward higher temperature direction.

With the increase of $MgSiO_3$ in the Fe–Ni–C system, it is found that the content of recrystallized flake graphite shown in Fig. 2(a) increases gradually in the catalyst system. This may be due to the incomplete absorption of the dissolved carbon source in the catalyst system.[31] The content of Fe–Ni metal

catalyst and graphite inclusions occurred in the diamond crystal shown in Figs. 2(b)–2(g) also increase gradually, and the inclusion content in the direction of [100] is much greater than that in the direction of [111]. For D-1, D-2, D-3 crystals doped with low-concentration $MgSiO_3$, the inclusions in Figs. 2(b) and 2(c) are distributed in single lines and dots along the [100] direction. As the concentration of doped $MgSiO_3$ increased to 2.0 wt%, the inclusions in Figs. 2(b), 2(d), and 2(e) exhibit a larger dot shape along the [100] direction and a linear distribution along the [111] direction. When the $MgSiO_3$ content is further increased to 3.0 wt%, the metal and graphite inclusions in Figs. 2(b), 2(f), and 2(g) further increase and show bead or tower distribution in the [100] direction and parallel dots and lines distribution in the [111] direction, respectively. The distribution of inclusions in diamond is related to the relative growth rate in the [111] and [100] directions. When the [100] direction grows too fast, the inclusions in the [100] direction will increase.[7] We speculate that the increase of inclusions in the [100] direction in the diamond crystals is related to the excessive growth in the [100] direction caused by the synergy of $MgSiO_3$ and the P–T diagram movement to the higher temperature direction.

The distribution pattern of different elements and corresponding phases was investigated by SEM-EDS mapping technology on the catalyst system of D-1 and D-5. The results are shown in Fig. 3. The synthesized diamond crystal is located at the centre of catalyst system shown in Figs. 3(a) and 3(g). For crystal D-1, Fe, Ni metal catalyst and recrystallized graphite are uniformly distributed in the outer layer next to the diamond shown in Figs. 3(e) and 3(f). For crystal D-5 with 3.0-wt% $MgSiO_3$ in Fe–Ni–C system, the outer layer next to the diamond is Fe, Ni metal catalyst shown in Figs. 3(k) and 3(l), while $MgSiO_3$, recrystallized graphite and Fe, Ni metal catalyst exist in the outer layer together (Fig. 3). The distribution pattern of diamond, recrystallized graphite, metal catalyst, and $MgSiO_3$ are in accordance with the observation as shown in Fig. 2(a).

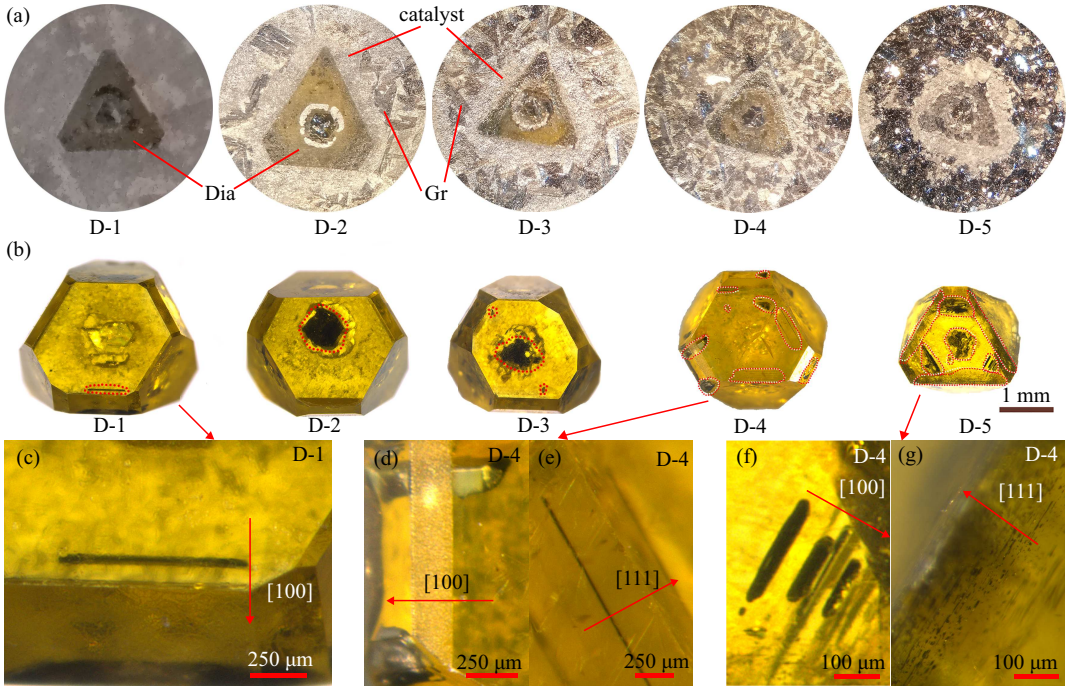

Fig. 2. The catalyst system and crystal characteristics of synthetic diamond doped with different contents $MgSiO_3$ in the Fe–Ni–C system. (a) The photos of catalyst system with 0.0-wt%, 1.0-wt%, 1.4-wt%, 2.0-wt%, 3.0-wt% $MgSiO_3$ doped before acid treatment. (b) Crystal photos of diamond synthesized by doping 0.0-wt% to 3.0-wt% $MgSiO_3$ in Fe–Ni–C system. The metal catalyst and graphite inclusions inside the crystal are shown by the red dotted line. (c)–(g) The inclusions distribution characteristics of D-1, D-4, and D-5 crystals. Dia: diamond. Gr: recrystallized graphite.

Table 1. Experiment conditions and diamond characteristics synthesized by doping 0.0-wt%–3.0-wt% $MgSiO_3$ in the Fe–Ni–C system.

Run	$MgSiO_3$/wt%	Temperature/°C	Weight/mg	Crystal morphology	Remarks
D-1	0.0	1385	31.7	{111} > {100} > {113} > {110}	l
D-2	1.0	1385	29.5	{111} > {100} > {113} > {110}	l
D-3	1.4	1385	28.5	{111} > {100} > {113} > {110}	l
D-4	2.0	1395	23.9	{111} > {100} > {113} > {110}	m
D-5	3.0	1405	16.7	{111} >> {110} > {100}	h

Here, l, m, h respectively represents the low, medium, and high contents of recrystallized graphite in the system.

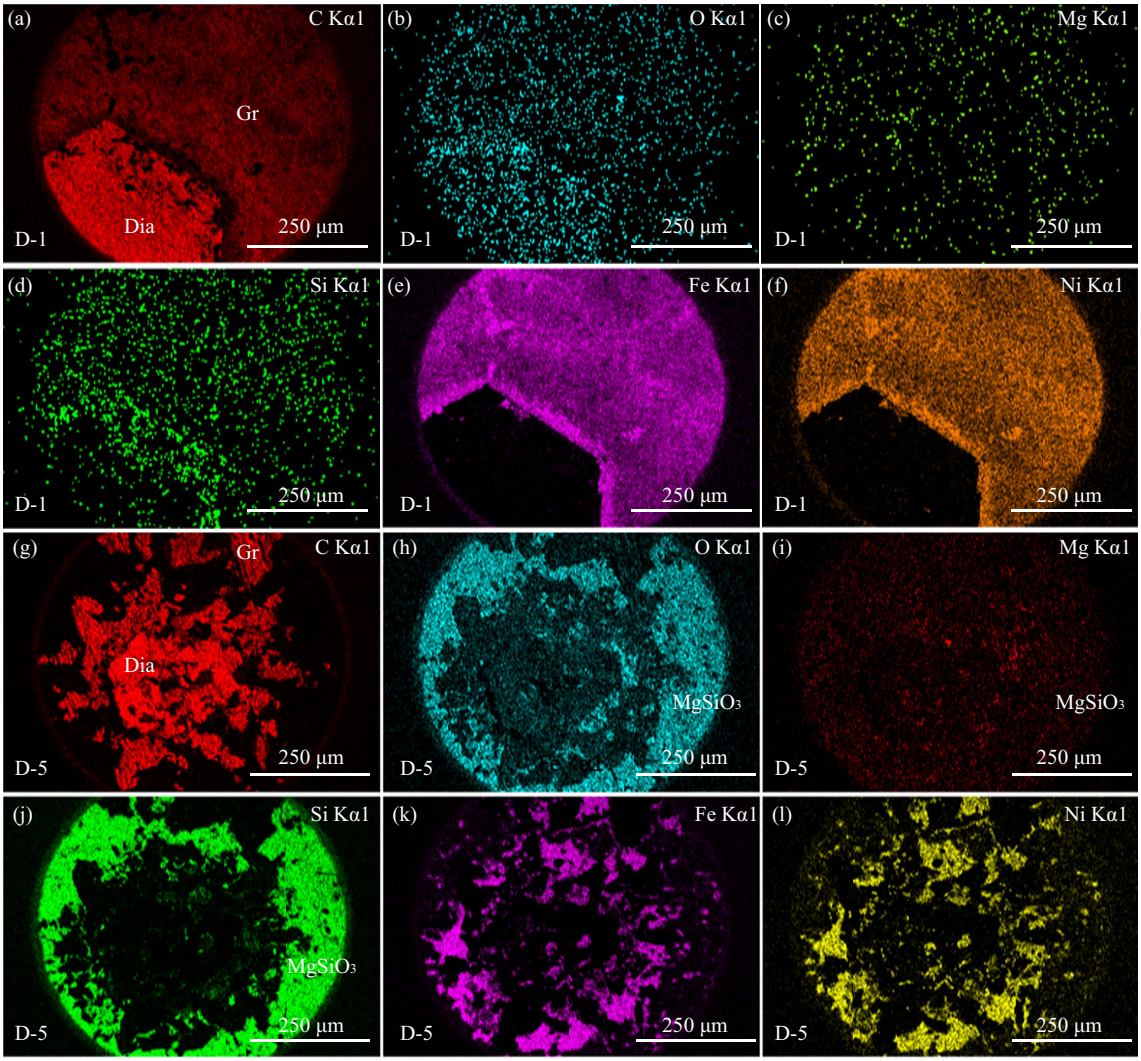

Fig. 3. The element distribution diagram of catalyst system obtained by SEM-EDS mapping technology on D-1 and D-5. (a)–(f) The distribution of C, O, Mg, Si, Fe, and Ni elements on D-1. (g)–(l) The distribution of C, O, Mg, Si, Fe, and Ni elements on D-5. Dia: diamond. Gr: recrystallized graphite.

3.2. Crystal morphology

In the Fe–Ni–C-$MgSiO_3$ system, the morphology of diamond crystals synthesized with {111} crystal as seed is shown in Table 1 and Fig. 4. Crystals D-1–D-4 with 0.0-wt% to 2.0-wt% $MgSiO_3$ doped are all the combination form of {111}, {100},

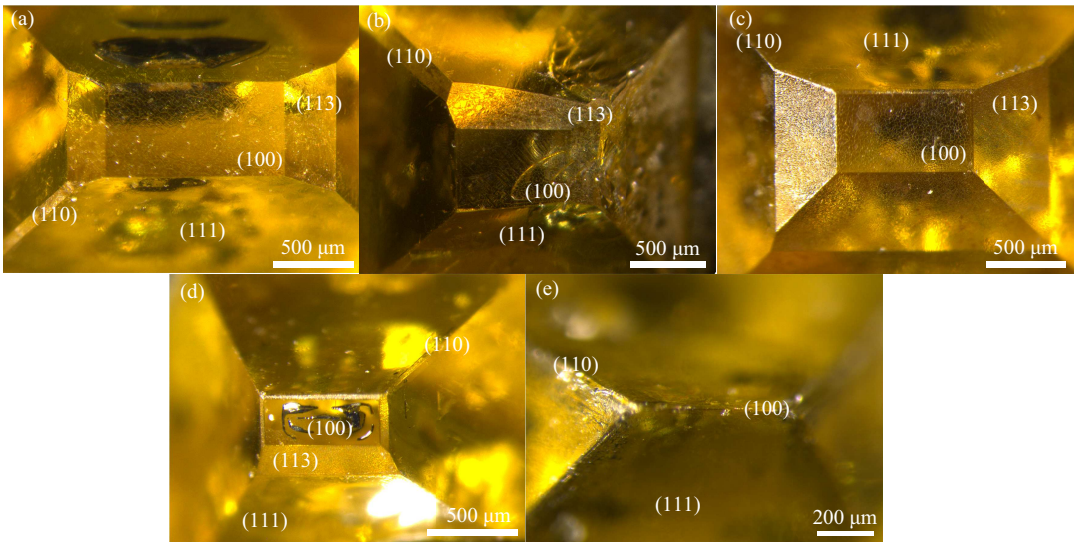

Fig. 4. The crystal characteristics of diamond synthesized by doping $MgSiO_3$ in the Fe–Ni–C system. (a)–(e) Crystal D-1 to D-5 synthesized by doping 0.0-wt%, 1.0-wt%, 1.4-wt%, 2.0-wt%, and 3.0-wt% $MgSiO_3$, respectively.

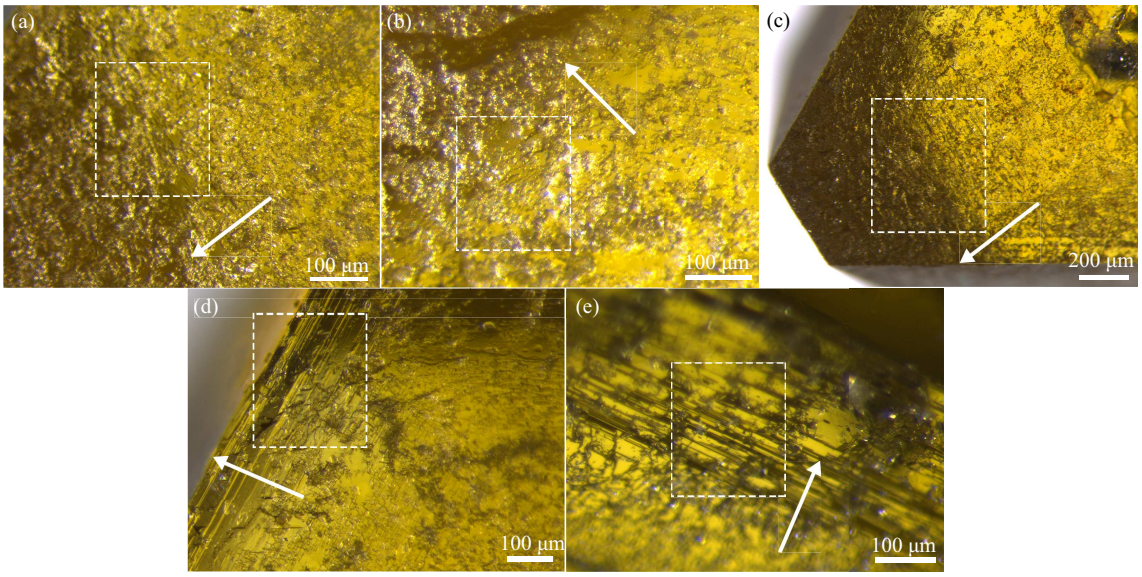

Fig. 5. The characteristics on the (111) crystal face at the bottom of the diamond crystals. (a)–(e) Crystal D-1–D-5 synthesized by doping 0.0-wt%, 1.0-wt%, 1.4-wt%, 2.0-wt%, and 3.0-wt% $MgSiO_3$, respectively. The arrows indicate the extension direction of the stepped growth layer from the centre of crystal to the edge.

{113}, {110} sectors and shows {111} > {100} > {113} > {110} regular pattern in Figs. 4(a)–4(d). Crystal D-5 with 3.0-wt% $MgSiO_3$ doped shows the combination form of {111}, {110}, {100} sectors, and the development of {111} sector in Fig. 4(e) is much better than {110} and {100} sectors. The (113) face of D-5 crystal has disappeared, and its (100) face is significantly smaller than that of D-1–D-4. It is concluded that with the increase of $MgSiO_3$ doping ratio, {100} and {113} sectors tend to decrease gradually, while {111} sector will gradually dominate the growth of diamond. This may also be ascribed to the higher growth rate in the [100] direction than in the [111] direction caused by the synergy of $MgSiO_3$ and the movement of *P*–*T* diagram toward higher temperature direction.

On the (111) crystal face at the bottom of the crystal, with the increase of $MgSiO_3$ from 0.0 wt% to 3.0 wt%, the step growth layer in Figs. 5(a)–5(e) changed gradually from not obvious to significantly visible. This evolution is interpreted by a higher dissolution rate in [100] and [113] directions than [111] direction of the micro-structure, so that the crystal face of the {111} sector can be retained.[32]

3.3. Crystal growth rate

Figure 6 shows the growth rate of diamond synthesized with different content of $MgSiO_3$ in the Fe–Ni–C system. The growth rate of D-1 with no $MgSiO_3$ addition is 1.4 mg/h. When the $MgSiO_3$ content increases to 1.0 wt% and 1.4 wt%, the corresponding crystal growth rate decreases to 1.3 mg/h and 1.2 mg/h, respectively. Furthermore, the growth rates of D-4 and D-5 with 2.0-wt% and 3.0-wt% $MgSiO_3$ doped are significantly reduced to 1.0 mg/h and 0.7 mg/h, respectively. The growth rate of diamond crystal decreases with the increase of the doped $MgSiO_3$ proportion. It is speculated that the synergy of $MgSiO_3$ and the increase of temperature could make the content of recrystallized graphite in the Fe–Ni–C system rise sharply and cause competition with carbon source needed for diamond growth, which results the decrease of crystal growth rate.[31,33]

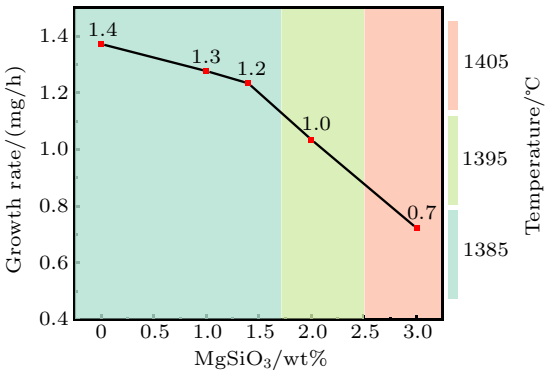

Fig. 6. Growth rate of diamond synthesized with 0.0-wt%–3.0-wt% $MgSiO_3$ doped in Fe–Ni–C system.

3.4. Infrared spectra

The infrared spectra of diamond crystals doped with 0.0-wt% to 3.0-wt% $MgSiO_3$ in the Fe–Ni–C system all contain 1130-cm^{-1} and 1344-cm^{-1} absorption peaks as shown in Fig. 7(a), which corresponds to single substitutional nitrogen (C form).[34–36] The following formula (1) was used to calculate the nitrogen content of C form (N_c). The error of N_c obtained in this way is less than 5%.[9,37,38]

$$\begin{aligned} N_c(\text{ppm}) &= \mu(1130\ \text{cm}^{-1})/\mu(2120\ \text{cm}^{-1}) \times 5.5 \times 25, \\ \mu(1130\ \text{cm}^{-1}) &= [A(1290\ \text{cm}^{-1}) - A(1370\ \text{cm}^{-1})]/0.31, \\ \mu(2120\ \text{cm}^{-1}) &= [40 \times A(2030\ \text{cm}^{-1}) \\ &\quad + 87 \times A(2160\ \text{cm}^{-1})]/127 - A(2120\ \text{cm}^{-1}). \end{aligned} \tag{1}$$

As shown in Fig. 7(b), the N_c of crystal D-1 with no

$MgSiO_3$ addition is 120 ppm, when $MgSiO_3$ is increased to 1.0 wt% and 1.4 wt%, the N_c of crystal D-2 and D-3 increase to 189 ppm and 190 ppm, respectively. Higher N_c about 216 ppm and 227 ppm occurs in the crystal D-4 and D-5 when $MgSiO_3$ is further increased to 2.0 wt% and 3.0 wt%, respectively. The addition of $MgSiO_3$ in the Fe–Ni–C system increases the nitrogen content in diamond crystal, it is explained by the enhancement that the poison of $MgSiO_3$ to Fe–Ni metal catalyst caused by the increase of $MgSiO_3$ content.[9] As a result, the solubility content of nitrogen in Fe–Ni metal decreases and increases the N_c in diamond. The high nitrogen content of natural diamond in the upper mantle may have a similar mechanism, the solubility of nitrogen in silicate is much lower than that in Fe–Ni–$MgSiO_3$ system under the condition of upper mantle temperature and pressure, which may makes the content of free nitrogen in the system increase to a higher level at average 235 ppm.[39]

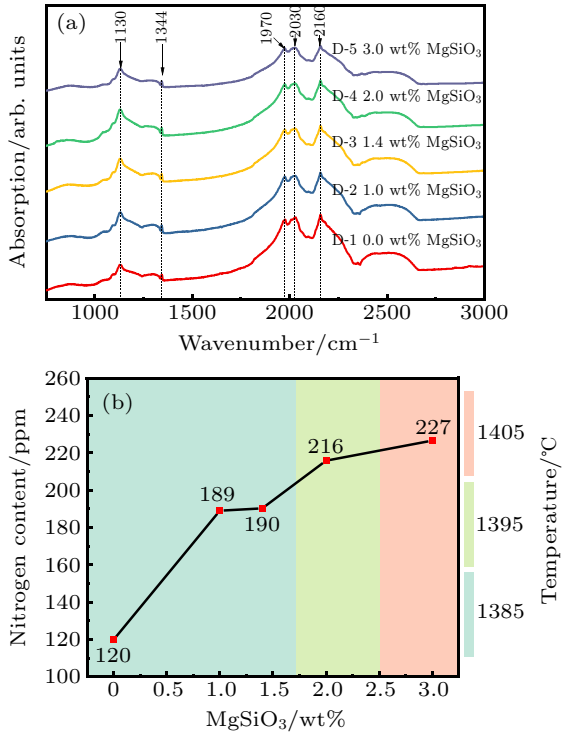

Fig. 7. Infrared spectra (a) and nitrogen content (b) of diamond synthesized with 0.0-wt%–3.0-wt% $MgSiO_3$ doped in the Fe–Ni–C system.

3.5. Raman spectra

Raman spectra of diamond doped with 0.0-wt%–3.0-wt% $MgSiO_3$ in the Fe–Ni–C system show a single strong and narrow diamond sp^3 vibration peak near the 1331 cm^{-1} in Fig. 8. It is noticed that the peak position of diamond in the Raman spectra gradually shifted from 1132.1 cm^{-1} to 1131.3 cm^{-1} with the increase of $MgSiO_3$ content. The following formula (2) was used to calculate the surface residual stress of diamond crystals synthesized with different $MgSiO_3$ doped:[40]

$$\sigma_h(\mathrm{GPa}) = [\gamma_0 - \gamma(\mathrm{cm}^{-1})]/2.88. \quad (2)$$

According to formula (2), the calculated positive stress corresponds to the residual tensile stress on the crystal surface. With the increase of $MgSiO_3$ content from 0.0 wt% to 3.0 wt% in the Fe–Ni–C system, the residual tensile stress on the crystal surface also rises from 0.0 GPa to 0.2 GPa (Table 2). The residual stress on the surface of synthetic diamond crystal is significantly affected by the content of metal inclusions in the crystal and increases with the amount of inclusions.[41] In Figs. 2(b)–2(g), we also observed that the content of metal inclusions in the crystals increased with the increase of $MgSiO_3$ doping content. The increase of residual tensile stress and the shift down of Raman peak position is related to the increase of inclusions inside the crystal.

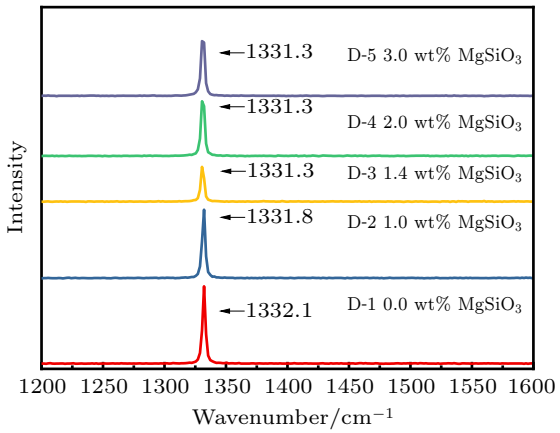

Fig. 8. Raman spectra of diamond crystals synthesized with 0.0-wt%–3.0-wt% $MgSiO_3$ doped in the Fe–Ni–C system.

Table 2. Raman shifts and stresses of diamond crystals synthesized with 0.0-wt%–3.0-wt% $MgSiO_3$ doped in the Fe–Ni–C system.

Run	$MgSiO_3$	Raman shift/cm^{-1}	$\Delta\gamma$/cm^{-1}	Stress/GPa
D-1	0.0	1332.1	-0.1	0.0
D-2	1.0	1331.8	0.2	0.1
D-3	1.4	1331.3	0.7	0.2
D-4	2.0	1331.3	0.7	0.2
D-5	3.0	1331.3	0.7	0.2

3.6. Influence of $MgSiO_3$ on type-Ib diamond synthesized in Fe–Ni–C system

Figure 9 summarizes the influence pattern of $MgSiO_3$ on type-Ib diamond synthesized in the Fe–Ni–C system. Firstly, it can be seen from the synthesis conditions shown in Table 1, under the same pressure condition, with the content of $MgSiO_3$ in the Fe–Ni–C system increases from 0.0 wt% to 3.0 wt%, the *P*–*T* diagram of diamond growth moves towards the direction of higher temperature, and this will affect many properties of the synthesized crystals. First, the increase of synthesis temperature from 1385 °C to 1405 °C will make the growth rate of diamond crystals in the [100] direction significantly faster than that in the [111] direction,.[7] This will eventually make the development of {111} sector in the crystal gradually dominant, while the development of {100} and {113} sectors slow down or even disappear.

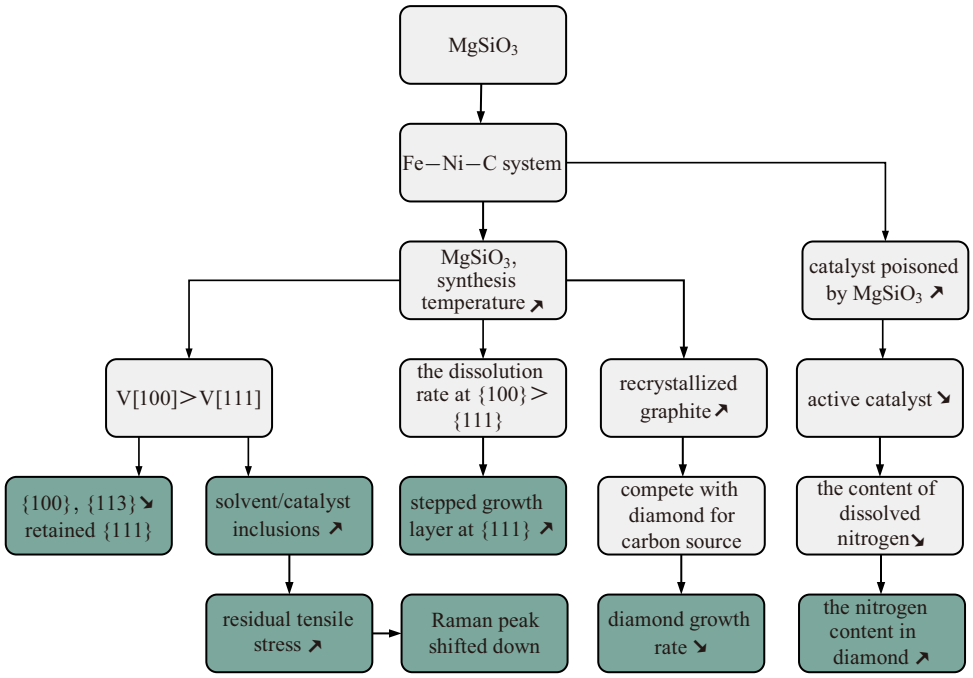

Fig. 9. Influence pattern of doped $MgSiO_3$ on diamond synthesized in the Fe–Ni–C system, the dark green frames are observed crystal characteristics.

In the interior of the crystal, because of the higher growth rate in the [100] direction than the growth rate in the [111] direction, it is easier for the metal catalyst and graphite in the synthetic system to enter the diamond crystal as inclusions and mainly distribute along the fast growing [100] direction. As the content of doped $MgSiO_3$ increases from 0.0 wt% to 3.0 wt% in the Fe–Ni–C system, the inclusions inside the diamond crystal gradually increase and evolve from the single dot or linear pattern to the parallel linear or beaded distribution pattern. Furthermore, the increased melt/catalyst and graphite inclusions increase the residual tensile stress on the synthetic diamond surface and shift the Raman peak position from 1132.1 cm^{-1} to 1131.3 cm^{-1}.[41] On the other hand, accompanying with the high growth rate, there is also a higher dissolution rate in the [100] direction than [111] direction.[32] The higher dissolution rate in the [100] direction may account for the micro-step growth layer structure on the bottom surface of (111).

The driving force of diamond synthesis by TGM method is the solubility difference between graphite and diamond in the metal solvent system. As the synthesis temperature increases, this driving force will gradually decrease to a certain extent that is too small to overcome the nucleate barrier for diamond. In this case, the carbon source dissolved in the Fe–Ni catalyst system exists in the form of metastable graphite and causes competition with carbon sources needed for diamond growth.[31] As a result, the growth rate of diamond crystals is significantly reduced from 1.4 mg/h to 0.7 mg/h.

The addition of $MgSiO_3$ in the Fe–Ni–C system has a toxic effect on the metal catalyst.[9] With the increase of $MgSiO_3$, the active Fe–Ni metal catalyst in the system is relatively lower (Fig. 3), and the amount of nitrogen dissolved in the system decreases,[42] as a result, the N_c of the synthesized crystal is increased. Polyanov *et al.* (2014) observed that the N_c of diamond grown under equilibrium condition in carbonate melt is higher than that of diamond grown in metal melt,[43] this phenomenon could be a similar mechanism to our work. The increased N_c in synthetic crystals may be caused by the poisoning of $MgSiO_3$ on catalyst.

The crystals D-1, D-2, and D-3 with 0.0-wt%, 1.0-wt%, 1.4-wt% $MgSiO_3$ doped were all synthesized at 1385 °C. D-4 and D-5 were synthesized at 1395 °C and 1405 °C, respectively. So, the effect of temperature can be discussed by comparing the evolution of D-1–D-3 and D-1–D-5, respectively. With the content of $MgSiO_3$ increasing from 0.0 wt% to 1.4 wt%, the growth rate decreased, the development of {111} sector gradually dominated, and the development of {100} and {113} sectors decreased. The nitrogen content also gradually increased, and the Raman shifts moved to the low wavenumber direction. The growth rate, crystal morphology, nitrogen content and Raman shift of D-1–D-3 were the same as those of D-1–D-5. Therefore, the influence of temperature can be excluded when separately discuss the effects of $MgSiO_3$ to the Fe–Ni–C system. the effects of $MgSiO_3$ to the Fe–Ni–C system are similar to that of temperature and significantly increase the growth rate and the accompanied dissolution rate at [100] direction than [111] direction. The addition of $MgSiO_3$ to the Fe–Ni–C system also increases the metastable graphite content and finally decreases the crystal growth rate. Thus, the observed crystal morphology and internal characteristics are the synergy of $MgSiO_3$ and the movement of the *P–T* diagram.

4. Conclusion and perspectives

In this paper, the effects of $MgSiO_3$ addition on the crystal morphology, internal and external structure, growth rate, and nitrogen content of type-Ib gem grade diamond under the condition of typical upper mantle temperature and pressure are discussed. The possible factors affecting the crystal structure and nitrogen content of the natural diamond produced by the upper mantle are also discussed.

With the increase of $MgSiO_3$ from 0.0 wt% to 3.0 wt% and the *P*–*T* diagram of diamond growth in the Fe–Ni–C system moves towards the direction of higher temperature, and its suitable growth temperature gradually increases from 1385 °C to 1405 °C, the synergy of $MgSiO_3$ and the movement of the *P*–*T* diagram results in the increase of recrystallized graphite content and the competition with the carbon source needed for the growth of diamond. Therefore, the crystal growth rate decreases from 1.4 mg/h to 0.7 mg/h.

Diamond crystals exhibit the combination form of {111}, {100}, {113}, {110} sectors, the increase of $MgSiO_3$ and the movement of the *P*–*T* diagram bring about a higher growth rate in [100] and [113] directions than [111] direction, as a result, {111} sector gradually dominate the morphology of diamond crystal. Besides, the higher growth rate in [100] direction forms the increased metal catalyst and graphite inclusions, thus leading to the increase of residual tensile stress on the crystal surface from 0.0 GPa to 0.2 GPa. Accompanying with the high growth rate, a higher dissolution rate occurs in the [100] direction than [111] direction and may account for the stepped growth layer on (111) face.

The addition of $MgSiO_3$ will poison the Fe–Ni catalyst in the system, resulting in a reduction of nitrogen dissolved in the system and the increase of the nitrogen content in the crystal. This also confirms the influence of the difference of redox environment between the upper mantle and the lower mantle on the average nitrogen content in the natural diamond.

Acknowledgment

The scientific contributions from other people or groups are acknowledged here. Financial supports are given in the footnote on the first page.

References

[1] Smith E M, Shirey S B and Wang W Y 2017 *Gems Gemol.* **53** 388
[2] Ogden J 2018 *Diamonds: An Early History of the King of Gems* (New Haven: Yale University Press) pp. 1–20
[3] Sally E M, Shigley J E and Breeding C M 2017 *Gems Gemol.* **53** 262
[4] Wang W Y, Moses T, Linares R C, Shigley J E, Hall M and Butler J E 2003 *Gems Gemol.* **39** 268
[5] Li Y, Wang Y, Li S S, Li Z B, Luo K W, Ran M W and Song M S 2019 *Acta Phys. Sin.* **68** 098101 (in Chinese)
[6] Fan X H, Xu B, Niu Z, Zhai T G and Tian B 2012 *Chin. Phys. Lett.* **29** 048102
[7] He X M, Du M Y, Zhang Y H, Chu P K and Guo Q F 2019 *JOM* **71** 2531
[8] Wang W Y and Moses T 2016 *Gems. Gemol.* **52** 101
[9] Liu X B, Jia X P, Zhang Z F, Li Y, Hu M H, Zhou Z X and Ma H A 2011 *Cryst. Growth Des.* **11** 3844
[10] Tian Y, Jia X P, Zang C Y, Li S S, Xiao H Y, Zhang Y F, Huang G F, Li R, Han Q G and Ma L Q 2009 *Chin. Sci. Bull.* **54** 1459
[11] Chen L C, Miao X Y, Ma H A, Guo L S, Wang Z K, Yang Z Q, Fang C and Jia X P 2018 *Crystengcomm* **20** 7164
[12] Huang G F, Jia H S, Li S S, Zhang Y F, Li Y, Zhao M and Ma H A 2010 *Chin. Phys. B* **19** 118101
[13] Smith E M, Kopylova M G, Frezzotti M L and Afanasiev V P 2015 *Lithos* **216** 106
[14] Stachel T and Luth R W 2015 *Lithos* **220** 200
[15] Dasgupta R and Hirschmann M M 2010 *Earth Planet. Sci. Lett.* **298** 1
[16] Cartigny P, Harris J W and Javoy M 2001 *Earth Planet. Sci. Lett.* **185** 85
[17] Pal'yanov Y N, Sokol A G and Sobolev N V 2005 *Russ. Geol. Geophys.* **46** 1271
[18] Sokol A and Pal'yanov Y N 2008 *Contrib. Mineral. Petrol.* **155** 33
[19] Fedortchouk Y, Liebske C and McCammon C 2019 *Earth Planet. Sci. Lett.* **506** 493
[20] Khokhryakov A F and Pal'yanov Y N 2010 *American Mineralogist* **95** 1508
[21] Palyanov Y N, Sokol A, Khokhryakov A and Kruk A 2015 *Russ. Geol. Geophys.* **56** 196
[22] Palyanov Y N, Kupriyanov I N, Khokhryakov A F and Borzdov Y M 2017 *Crystengcomm* **19** 4459
[23] Ding L Y, Ma H A, Fang S, Yang Z Q, Chen L C, Wang F B and Jia X P 2020 *J. Cryst. Growth* **533** 125463
[24] Palyanov Y N, Sokol A G, Tomilenko A A and Sobolev N V 2005 *Eur. J. Mineral.* **17** 207
[25] Shatskiy A, Borzdov Y M, Sokol A G, Katsura T and Palyanov Y N 2008 *International Kimberlite Conference: Extended Abstracts*, Shatskiy A, Borzdov Y M, Sokol A G, Katsura T and Palyanov Y N 2008 International Kimberlite Conference: Extended Abstracts, August 10–15, 2008, Frankfurt, Germany, p. 1
[26] Bataleva Y, Palyanov Y, Borzdov Y, Novoselov I and Bayukov O 2018 *Minerals* **8** 522
[27] Jacob D, Kronz A and Viljoen K 2004 *Contrib. Mineral. Petrol.* **146** 566
[28] Bulanova G 1995 *J. Geochem. Explor.* **53** 1
[29] Garanin V and Kudryavtseva G 1990 *Lithos* **25** 211
[30] Zedgenizov D, Bogush I, Shatsky V, Kovalchuk O, Ragozin A and Kalinina V 2019 *Minerals* **9** 741
[31] Zang C Y, Jia X P, Ma H A, Tian Y and Xiao H Y 2005 *Chin. Phys. Lett.* **22** 2415
[32] Fedortchouk Y and Canil D 2009 *Eur. J. Mineral.* **21** 623
[33] Hao Z Y, Chen Y F and Chen L Z 1994 *J. Cryst. Growth* **135** 370
[34] Smith W, Sorokin P, Gelles I and Lasher G 1959 *Phys. Rev.* **115** 1546
[35] Fallon P, Brown L, Barry J and Bruley J 1995 *Philos. Mag. A* **72** 21
[36] Liang Z Z, Jia X P, Ma H A, Zang C Y, Zhu P W, Guan Q F and Kanda H 2005 *Diam. Relat. Mat.* **14** 1932
[37] Fang S, Ma H A, Cai Z H, Wang C X, Fang C, Zhao Z D, Lu Z Y, Wang Y K, Chen L C and Jia X P 2020 *Crystengcomm* **22** 602
[38] Palyanov Y N, Borzdov Y M, Kupriyanov I N and Khokhryakov A F 2012 *Cryst. Growth Des.* **12** 5571
[39] Mysen B 2019 *Prog. Earth Planet. Sci.* **6** 1
[40] Catledge S A, Vohra Y K, Ladi R and Rai G 1996 *Diam. Relat. Mat.* **5** 1159
[41] Jia H S, Ma H A, Guo W and Jia X P 2010 *Sci. China-Phys. Mech. Astron.* **53** 1445
[42] Burns R, Hansen J, Spits R, Sibanda M, Welbourn C and Welch D 1999 *Diam. Relat. Mat.* **8** 1433
[43] Palyanov Y N, Bataleva Y V, Sokol A G, Borzdov Y M, Kupriyanov I N, Reutsky V N and Sobolev N V 2013 *Proc. Natl. Acad. Sci. USA* **110** 20408